Journal of Hazardous Materials 186 (2011) 197–205

Contents lists available at ScienceDirect

Journal of Hazardous Materials

journal homepage: www.elsevier.com/locate/jhazmat

Selective adsorption behavior of Pb(II) by mesoporous silica SBA-15-supported Pb(II)-imprinted polymer based on surface molecularly imprinting technique

Yan Liu[a], Zhanchao Liu[b], Jie Gao[a], Jiangdong Dai[a], Juan Han[a], Yun Wang[a], Jimin Xie[a], Yongsheng Yan[a,*]

[a] School of Chemistry and Chemical Engineering, Jiangsu University, XueFu Road 201#, Zhenjiang 212013, China
[b] School of Materials Science and Engineering, Jiangsu University of Science and Technology, Zhenjiang 212013, China

ARTICLE INFO

Article history:
Received 16 July 2010
Received in revised form 22 October 2010
Accepted 27 October 2010
Available online 4 November 2010

Keywords:
SBA-15
Surface ion-imprinted
Pb(II)
Adsorption
Selective

ABSTRACT

In this study, a new Pb(II) ion-imprinted polymer (Pb(II)-IIP), which can be used for selective adsorption of Pb(II) from aqueous solutions, was successfully prepared based on the supported material of ordered mesoporous silica SBA-15 with the help of surface molecular imprinting technology. The prepared polymer was characterized by Fourier transmission infrared spectrometry, X-ray diffraction, transmission electron microscope and nitrogen adsorption–desorption isotherm. The results showed that the synthesized polymer possessed high ordered mesoporous structure. The adsorption behavior of the adsorbents for Pb(II) was investigated using batch experiments. The Pb(II)-IIP showed fast kinetics, high selectivity and satisfied adsorption capacity for adsorption of Pb(II). Under the optimum experimental condition, Pb(II) adsorption process over Pb(II)-IIP follows pseudo-second-order reaction kinetics and follows the Langmuir adsorption isotherm. In addition, the thermodynamic parameters calculated from the adsorption data suggested that the adsorption of Pb(II) onto Pb(II)-IIP was a spontaneous and exothermic nature of the process.

1. Introduction

Lead is an important compound used as an intermediate in the processing industries such as plating, paint and dyes, and lead batteries [1]. Through the food chain system of soil–plant–animal–human, Pb(II) is transferred into animals and human beings [2]. Therefore, the development of reliable methods for the removal of lead is of particular significance [3]. However, the direct analysis of Pb(II) is often disturbed because of the presence of complex matrix in the environmental samples [4]. Consequently, the selective separation of Pb(II) from natural samples needs much more attention.

Solid-phase extraction (SPE) is one of the most used techniques for separation of selected analytes due to its flexibility, environmental-friendly, and simplicity [5]. However, the basic disadvantage of traditional SPE adsorbents is lack of selectivity for metal ions [6], which leads to the interference of other species for the determination of the target metal ions. Recently, it was extensively reported that the selectivity of SPE can be enhanced by using molecularly imprinted polymer (MIP), which have synthetic recognition sites with high selectivity and affinity for the template [7]. Ion imprinting polymer (IIP) is similar to MIP, but they recognize metal ions. A particular promising application of IIP is the SPE separation from other coexisting ions [8]. IIP has the outstanding advantages of predetermined selectivity, simplicity and convenience to prepare. However, traditional IIP exhibits poor site accessibility to the target molecules due to the functionality are totally embedded by high cross-linking density in the polymer matrices. Nowadays, efforts have been made to deal with the issue of accessibility by imprinting on matrix surfaces [9,10]. Surface molecularly imprinted polymer not only features high selectivity but also has many advantages: the sites are more accessible, and the binding kinetics is faster [11].

Surface-imprinting technique involves the emulsion polymerization utilizing a functional monomer, an emulsion stabilizer, a polymer matrix-forming comonomer and a print molecule. An important kind of surface imprinting technique is based on the surface modification of the matrix material. The distribution of the imprinted cavities in the thin polymer layer on matrix material is of great advantage to the fast binding of the template molecules with the recognition sites. The synthesis process can be explained generally as follows: (1) template molecules graft on functional monomer until reaching saturation; (2) post-imprinting of template molecules is conduced towards the grafted polymers using cross-linking agent; (3) the polymer grafts on the surface of matrix material and forms a thin polymer layer [12].

Silica based materials are common supports because they are stable under acidic conditions and no swelling inorganic material, and has high mass exchange characteristics [13]. In recent years, silica based mesoporous materials have been universally reported as

* Corresponding author. Tel.: +86 0511 88790683.
E-mail address: lyan@ujs.edu.cn (Y. Yan).

0304-3894/$ – see front matter © 2010 Elsevier B.V. All rights reserved.
doi:10.1016/j.jhazmat.2010.10.105

good solid support due to their stable mesoporous structure, good chemical and mechanical stability, and well modified surface properties with abundant Si-OH active bonds on the pore walls [14]. For adsorption application, the removal efficiency of heavy metal ions increases remarkably after the mesoporous silica has been modified by the functional groups [15–19]. Commonly, the mesoporous silica can be modified by the post-synthesis or one-pot synthesis. Especially the post-synthesis method does not destroy the mesoporous structural ordering, but functional groups are anchored on the surface or inside the pores of the mesoporous silica [20]. Among the mesoporous silicas, SBA-15 is characterized with highly ordered two-dimensional symmetry possesses hexagonal arrays of uniform pores with ultra large pore diameters, large surface area, high pore volume and thicker pore walls. It also shows excellent homogeneity and chemical/mechanical stability [21,22]. These characteristics of SBA-15 enables itself a potential candidate for inclusion of guest species on the surface. To the best of our knowledge, there has been no report focused on surface IIP synthesized by support of SBA-15.

Chitosan (CTS) is the N-deacetylated products of chitin that is the second most abundant natural biopolymer after cellulose. As an abundantly available low-cost adsorbent, this natural polymer and the derivatives have received great attention in the application of metal adsorption due to the high ratio of hydroxyl groups and amine groups [23]. However, the poor mechanical and chemical stability of pure CTS limits the application [24]. Many chemical modifications have been applied to improve the physical and chemical properties of CTS. Coating chitosan on preformed microparticle, e.g., silica gel with chemical cross-linking process has shown a successful method [25,26]. The essence lies in the combination of the functionality of chitosan and advantages of silica gel, e.g., large surface area and excellent mechanical resistance.

In this study, we synthesized a novel Pb(II)-IIP using CTS as functional monomer on support matrix of SBA-15 by surface imprinted technology. The structural characteristics, adsorption behavior of the Pb(II)-IIP adsorbents towards Pb(II) in aqueous solution were described and discussed in detail.

2. Experimental

2.1. Chemicals

CTS, degree of deacetylation more than 90% (Guoyao Chemical Reagents Corp., Shanghai, China), silane coupling agent KH-560 (γ-(2,3-epoxypropoxy)propyltrimethoxysilane) (Nanjing Shuguang Chemical Corp., Nanjing, China), Pluronic P123, triblock poly(ethylene oxide)–poly(propylene oxide)–poly(ethylene oxide), ($EO_{20}PO_{70}EO_{20}$, molecular weight 5800) (Sigma, USA) were used in our work. Standard stock solution of Pb(II) (1.0 g/L) was prepared by dissolving $Pb(NO_3)_2{\cdot}6H_2O$. All the chemicals used were of analytical grade. Doubly distilled water (DDW) was used for all dilutions.

2.2. Apparatus and measurements

Spectrometric measurements were carried out with a TAS-986 flame atomic adsorption spectrometer (FAAS) (Beijing, China). Fourier transmission infrared spectra (FT-IR, 4000–400 cm^{-1}) in KBr were recorded on a NICOLET NEXUS 470 FT-IR spectrometer (Nicolet, USA). Low-angle X-ray powder diffraction (XRD) measurements were carried out with a Bruker D8 diffractometer (Bruker, Germany) using a wavelength of 1.5418 Å (Cu K_α) and an angle of 0.5–10° with 0.002° steps. Transmission electron microscope (TEM) analysis was performed by using JEM-2010HR at 200 kV (JEOL, Japan,). A NOVA2000 surface area and pore size analyzer (Quntachrome, USA) measured surface area and pore size distribution. Brunauer–Emmett–Teller (BET) and Barrett–Joyner–Halenda (BJH) method were employed to calculate the surface area and pore diameter. The particles size was tested by BI-9000 high concentrations of laser particle size analyzer (Brook Haven, USA).

2.3. Preparation of Pb(II)-IIP

SBA-15 was synthesized as described by Zhao et al. [27]. It was activated with 3 mol/L hydrochloric acid by refluxing for 24 h, then washed and dried. The activated SBA-15 was obtained.

4.0 g of CTS and 0.4 g of $Pb(NO_3)_2{\cdot}6H_2O$ were dissolved in 160.0 mL of 0.1 mol/L HAc aqueous solution and stirred constantly for 1 h. Then, 40.0 mL of KH-560 as cross-linking agent was added into the transparent solution. The mixture was stirred for 4 h and then bathed in an ultrasonic bath for 20 min in order to make solution entirely dispersed. Finally, added 16.6 g of activated SBA-15 into the above polymer, and continue stirring for 2 h until the polymer loaded onto carrier well. Then the dry product was grinded and treated with 2.0 mol/L HCl to completely leach the coordinated and non-coordinated Pb(II). At last, the polymer was filtered with DDW to neutralization, dried at 60 °C under vacuum, grinded and sifted with 100 meshes screen. By comparison, the non-imprinted polymer (NIP) was also prepared as a blank in parallel but without the addition of $Pb(NO_3)_2{\cdot}6H_2O$.

2.4. Adsorption experiments

2.4.1. Pb(II) adsorption batch experiments

Adsorption of Pb(II) from aqueous solutions was investigated in batch experiments. 0.05 g of Pb(II)-IIP was added into 25.0 mL colorimetric tube containing certain amount of Pb(II) at a pH value of 6.0 (adjusted with 0.1 mol/L HCl and 0.1 mol/L $NH_3{\cdot}H_2O$) at 25 °C. Then the mixture was shaken vigorously for 10 min, the adsorption time was maintained for certain moment. After centrifugation, the concentration of Pb(II) in the residues solution was determined by FAAS. The adsorption ratio (E%), absorption capacity q_e (mg/g) at equilibrium, and adsorption amount at time t (min) q_t (mg/g) were calculated as follows:

$$E = \frac{C_0 - C_e}{C_0} \times 100\% \quad (1)$$

$$q_e = \frac{(C_0 - C_e)V}{W} \quad (2)$$

$$q_t = \frac{(C_0 - C_t)V}{W} \quad (3)$$

where C_0 (mg/L), C_e (mg/L) and C_t (mg/L) are concentrations of Pb(II) at initial, equilibrium and time t, respectively. V (mL) and W (g) are the volume of solution and the mass of sorbent, respectively.

2.4.2. Selectivity study

In order to measure the selectivity of the imprinted polymer, competitive adsorption of Pb(II)/M (M: other metal ions) and from their mixtures were investigated by using SBA-15, Pb(II)-IIP and NIP, respectively. The distribution coefficient K_d (mL/g), selectivity coefficient k, and the relative selectivity coefficient k' [28] were given as follows:

$$K_d = \frac{(C_i - C_f)V}{C_f W} \quad (4)$$

$$k = \frac{K_d}{K_d} \quad (5)$$

$$k' = \frac{k_{(\mathrm{IIP})}}{k_{(\mathrm{NIP})}} \quad (6)$$

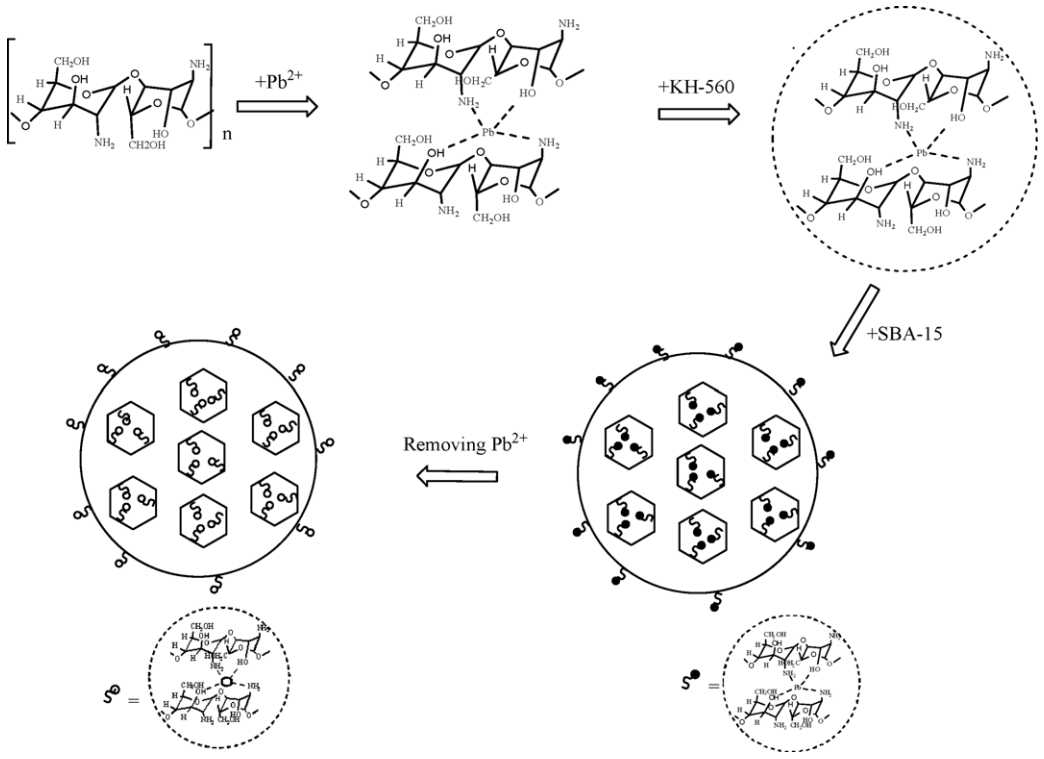

Fig. 1. Schematic illustration of preparation process of Pb(II)-IIP supported by SBA-15.

C_i and C_f represent the initial and equilibrated concentrations of the given metal ions in solution, respectively. $K_{d(Pb)}$ and $K_{d(M)}$ represent the distribution coefficient of Pb(II) and M ions respectively. $k_{(IIP)}$ and $k_{(NIP)}$ represent the selectivity coefficient of Pb(II)-IIP and NIP, respectively.

3. Results and discussion

3.1. Preparation

The synthesis of Pb(II)-IIP can be classified into the following four approaches as shown in Fig. 1: (1) linear chain CTS carrying metal-binding groups (–OH, $–NH_2$) chelated with Pb(II); (2) coordinated complexes immobilization by polymerization of KH-560, forming a cross-linked polymer network; (3) surface imprinting conducted on SBA-15 interface by co-condensation of Si-OH and –OH on KH-560; (4) removing chelated Pb(II) by HCl. The imprinted functionalized SBA-15 sorbent which contained predetermined orientation and tailor-made cavities on surface for Pb(II) was formed. During the synthesis process, on the one hand, KH-560 reacted onto CTS chains through the acid-catalyzed amino-oxirane addition reaction in the acidic aqueous solution; On the other hand, SBA-15 reacted with silantriol groups in KH-560 to form covalently bound surface monolayers of the metal alkoxide.

3.2. Characterization

3.2.1. FT-IR results

The FT-IR spectra of the samples were shown in Fig. 2. The wide and strong adsorption band at 3445 cm^{-1} ascribes to stretching vibrations of N–H and O–H in CTS [29,30]. But this characteristic absorption bands shifted to 3433 cm^{-1} (Fig. 2, trace b) due to –N and –O coordination with Pb(II). Bending vibration of $–NH_2$ at 1650 cm^{-1}, stretching vibrations of –OH at 1153 cm^{-1} and 1088 cm^{-1} in CTS shifted to 1557 cm^{-1}, 1085 cm^{-1} and 1014 cm^{-1}, respectively (Fig. 2, trace b), approving complex of Pb–N and Pb–O.

KH-560 is an epoxy-siloxane with trimethoxy anchor groups, and the peak for Si–O–C is at 1080 cm^{-1}. The peaks at 2960 cm^{-1}

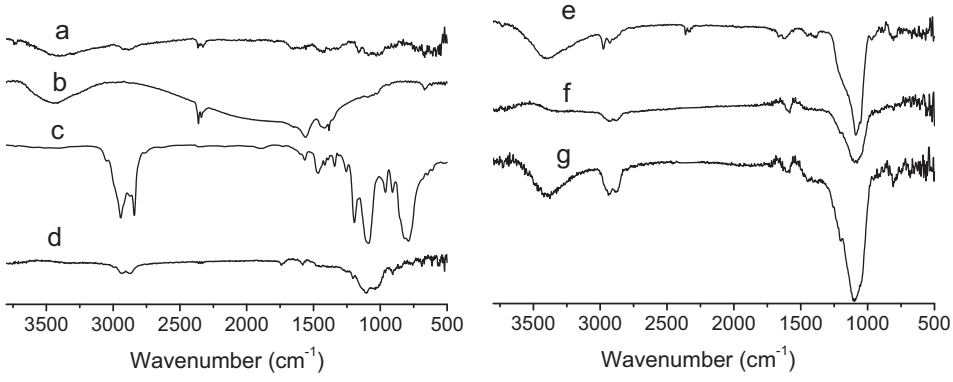

Fig. 2. FT-IR spectra: (a) CTS; (b) CTS-Pb(II); (c) KH-560; (d) Pb(II)-CTS/KH-560; (e) SBA-15; (f) Pb(II)-IIP unleached of Pb(II); (g) Pb(II)-IIP.

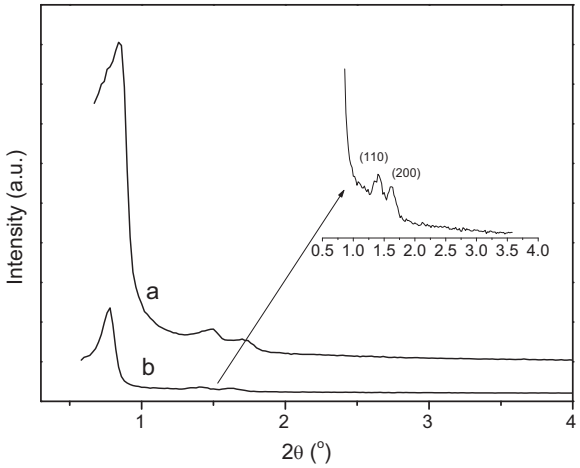

Fig. 3. XRD patterns: (a) SBA-15; (b) Pb(II)-IIP. Insert: enlarged patterns of (b) for the apparent observation.

and 2850 cm^{-1} attribute to stretching vibrations of $-CH_3$, and the peak at 770 cm^{-1} is assigned to epoxy group. Compared with KH-560, the peak intensity of $-CH_3$ declined and the characteristic feature of epoxy group vanished in Fig. 2, trace d. Moreover, typical Si–O–Si band around 1090 cm^{-1} was present as well. These results confirmed that KH-560 successfully linked with complex from CTS-Pb(II) accompany with ring-opening process, resulting in the desired high degree Si–O–Si network [21].

The absorption bands of mesoporous SBA-15 at 803 cm^{-1}, 1085 cm^{-1} characterize the stretching vibration, anti-symmetric stretching vibration of Si–O tetrahedron, respectively. The absorption at 1617 cm^{-1} attributes to inplane bending vibration of Si-OH. The broad absorption peak at 3440 cm^{-1} can be considered as variety vibration absorption of surface Si-OH. Co-condensation between silanols from self-hydrolysis of siloxane and SBA-15 took place, as a result overlapped peak of Si–O–Si from cross-linking reaction and condensation obtained in Fig. 2, trace f.

When compared unleached (Fig. 2, trace f) and leached imprinted sorbents (Fig. 2, trace g), it was found that the spectra of O–H and N–H bands were recovered and became sharper after removal of Pb(II). It suggested that the template ions were removed from the imprinted polymer sorbent.

3.2.2. XRD, TEM and nitrogen adsorption–desorption characterization

Powder XRD patterns results are shown in Fig. 3. Three XRD peaks at 0.85°, 1.50° and 1.72° were observed for Pb(II)-IIP, which corresponded to the (1 0 0), (1 1 0) and (2 0 0) reflections of SBA-15 [27], respectively, suggesting that the structure of SBA-15 was well preserved. The decrease in the (1 0 0) XRD diffraction peak in Pb(II)-IIP provided evidence that grafting mainly occurs inside the mesopore channels, since the attachment of organic functional groups in the mesopore channels tends to reduce the scattering power of the mesoporous silicate wall [31].

Table 1
Pore characterization of SBA-15, Pb(II)-IIP unleached and Pb(II)-IIP.

Samples	Surface area (m^2/g)	Pore volume (cm^3/g)	Average pore diameter (nm)
SBA-15	546.03	0.82	6.6
Pb(II)-IIP unleached	100.82	0.12	2.6
Pb(II)-IIP	113.81	0.27	3.9

Table 1 summarizes the physical parameters for SBA-15 and polymer that calculated from nitrogen adsorption–desorption isotherms. After polymerization, the surface area, total pore volume and BJH average pore diameter decreased, respectively, this was due to grafting occurred on the mesoporous channel. The leached Pb(II)-IIP showed a little increase of the three parameters which can be attributed to the presence of the cavities after leached of Pb(II) ions.

As shown in Fig. 4, well-ordered hexagonal array of mesopores were observed for both pure siliceous SBA-15 and Pb(II)-IIP when the electron beam was parallel to the main axis of the mesopores [32]. It was consistent with the results of XRD, indicating that the ordered mesoporous structure of the SBA-15 was well maintained after grafting. The average pore size of SBA-15 was ca. 6.4 nm, which was very close to the value (6.6 nm) determined by nitrogen adsorption. Fig. 4b showed that the pores were partly filled with polymer, in which a pore diameter of ca. 3.5 nm at the pore entrance can be seen. The pore diameters obtained for the two samples were in good agreement with the BET results. It was evident that the imprinting process did not destroy the ordered meso-structure and the graft mainly occurred on the mesopore channels.

3.3. Adsorption experiments

3.3.1. Effect of pH and mass of sorbent

The effect of pH on the adsorption process is presented in Table 2. Since precipitation occurred, the pH higher than 7 was not investigated. With increasing pH value, the competition from the hydrogen ions decreased and Pb(II) ions can be adsorbed on the adsorbent [33]. The adsorption ratio has reached more than 95% at pH 6. Subsequently, initial pH value of 6 was selected as the experimental pH.

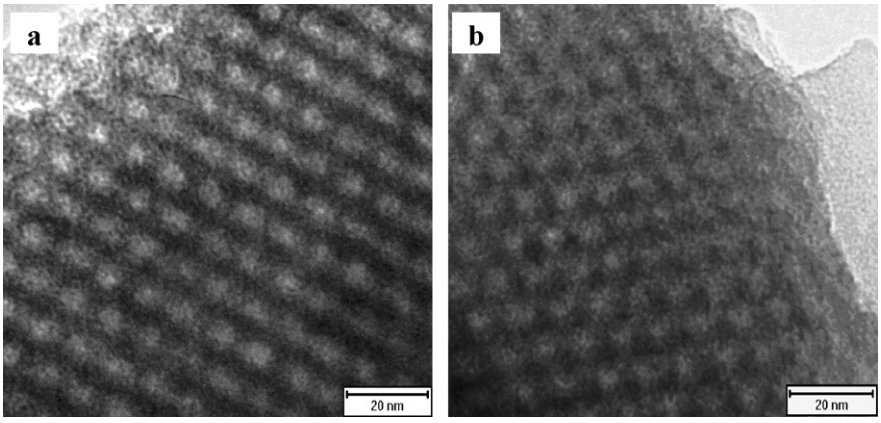

Fig. 4. TEM of (a) SBA-15; (b) Pb(II)-IIP with the electron beam parallel to the pore channels.

Table 2
Effect of initial pH and mass of sorbent on adsorption of Pb(II) onto Pb(II)-IIP.

pH	Adsorption ratio (%)	Mass of sorbent (g)	Adsorption ratio (%)
1	6.00	0.01	92.67
2	9.00	0.05	97.00
3	16.33	0.08	97.33
4	22.00	0.10	97.67
5	36.33	0.16	97.67
6	97.67	0.20	97.67
7	98.00	0.30	97.67
		0.40	98.00

As shown in Table 2, the adsorption ratio of Pb(II)-IIP towards Pb(II) reached more than 97% at higher masses more than 0.05 g. So 0.05 g was chosed as the optimum mass of sorbent.

3.3.2. *Effect of contact time at different initial ion concentrations and temperatures*

A study of the effect of contact time on the adsorption of Pb(II) at different initial concentrations and temperatures were shown in Fig. 5. It was observed that the adsorption rate was high from *t*: 0 to about 30 and became slow during the latter stages. The adsorption processes reached equilibrium less than 90 min for all the initial concentrations and temperatures studied. The value of present work was lower than that of NIP (150 min), or reported in the literature where the saturated adsorption time was found to be near 10 h for Pb(II) adsorption on sol–gel processing molecular imprinted polymer [34], or 6 h for the adsorption on thiourea-modified chitosan resin imprinted polymer [35]. This result could be due to the homogeneous distribution of active sites on the surface of Pb(II)-IIP. With changing the concentration of the solution from 3.0 mg/L to 8.0 mg/L, the absolute amount of Pb(II) ions per unit of adsorbent increased from 0.74 mg/g to 1.88 mg/g at 25 °C. When increasing temperature from 15 °C to 35 °C, the absorbed amount slightly decreased from 0.75 mg/g to 0.68 mg/g. It indicated that low temperature was in favour of removal. However, the adsorbed amount on NIP increased from 0.32 mg/g to 0.38 mg/g with increasing temperature from 15 °C to 35 °C. It indicated that high temperature was in favour of adsorption.

3.3.3. *Kinetics studies*

To evaluate the adsorption kinetics of Pb(II) ions, two different kinetic models were applied for the experimental data [36]:

The pseudo-first-order equation is:

$$\ln(q_e - q_t) = \ln q_e - k_1 t \tag{7}$$

The pseudo-second-order equation is:

$$\frac{t}{q_t} = \frac{1}{k_2 q_e^2} + \left(\frac{1}{q_e}\right) t \tag{8}$$

q_e (mg/g) and q_t (mg/g) are the adsorption capacity at equilibrium and the adsorption amount at time t (min), respectively. q_e values calculated from the intercept of plot $\ln(q_e - q_t)$ vs. t and the slope of t/q_t vs. t are defined as theoretical $q_{e(\mathrm{cal})}$ value of pseudo-first-order and pseudo-second-order model, respectively. k_1 (min^{-1}) and k_2 (mg/g min) are pseudo-first-order and pseudo-second-order rate constants of adsorption, respectively.

Pseudo-first-order model is rendered the rate of occupation of the adsorption sites to be proportional to the number of unoccupied sites; pseudo-second-order kinetic model is assumed the chemical reaction mechanisms [37], and that the adsorption rate is controlled by chemical adsorption through sharing or exchange of electrons between the adsorbrate and adsorbent [38]. Parameters of two kinetic models are given in Table 3. The best-fit model was selected based on both linear regression correlation coefficient (R^2) and the theoretical $q_{e(\mathrm{cal})}$ value. The pseudo-second-order rate equation for adsorption of Pb(II) ions onto Pb(II)-IIP agreed well with the data for $R^2 = 0.998$. In addition, the theoretical $q_{e(\mathrm{cal})}$ values were closer to the experimental $q_{e(\mathrm{exp})}$. It can be said that the pseudo-second-order kinetic model provided a good correlation for the adsorption of Pb(II) onto Pb(II)-IIP in contrast to the pseudo-first-order model. Therefore, the adsorption behavior of Pb(II) onto Pb(II)-IIP belonged to the pseudo-second-order kinetic model and the adsorption process was a chemical process. As indicated in Table 3, Pb(II) adsorption onto NIP belonged to the pseudo-second-order kinetic model too, but k_2 followed the order Pb(II)-IIP > NIP. The fast binding of the template ion was attributed to high affinity recognition sites on NIP.

To gain insight into the mechanism and rate-controlling steps affecting the kinetics of adsorption, intraparticle diffusion and external mass transfer have been applied to investigate the adsorption process.

Intraparticle diffusion equation was given as cited in [3]

$$q_t = k_d t^{1/2} + y \tag{9}$$

q_t (mg/g) is the amount of metal ions adsorbed at time t, K_d ($\mathrm{mg/L\,min^{-0.5}}$) is the initial rate of intraparticular diffusion and y is the intercept. Value of y gives information on to the thickness of the boundary layer, that is, the larger the intercept, the greater the boundary-layer effect.

The liquid film diffusion model namely external mass transfer may be applied to determine the transport of the solute molecules

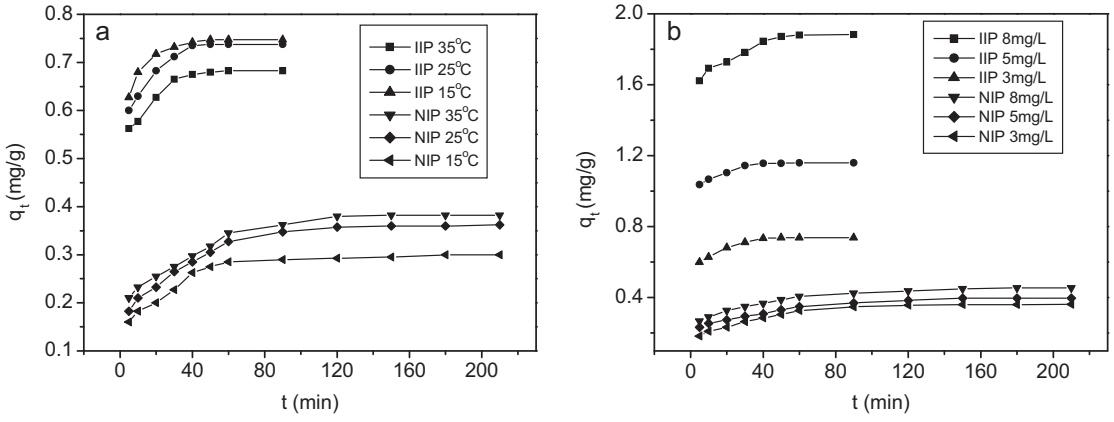

Fig. 5. Effect of time on the adsorption of Pb(II) onto Pb(II)-IIP and NIP at (a): different initial concentrations; (b) different temperatures.

Table 3
Pseudo-first-order, pseudo-second-order kinetics parameters for adsorption of Pb(II) onto Pb(II)-IIP and NIP.

	Parameter	$q_{e(exp)}$ (mg/g)	Pseudo-first-order kinetics			Pseudo-second-order kinetics		
			$q_{e(cal)}$ (mg/g)	k_1 (min^{-1})	R^2	$q_{e(cal)}$ (mg/g)	k_2 (g/mg min)	R^2
Pb(II)-IIP	Temp. (°C)							
	15	0.75	0.085	5.05×10^{-2}	0.830	0.76	1.30	0.999
	25	0.74	0.123	5.62×10^{-2}	0.806	0.75	0.84	0.999
	35	0.68	0.169	7.51×10^{-2}	0.915	0.70	0.88	0.999
	C_0 (mg/L)							
	3.0	0.74	0.123	5.62×10^{-2}	0.806	0.75	0.84	0.999
	5.0	1.16	0.127	1.74×10^{-2}	0.723	1.17	1.03	0.999
	8.0	1.88	0.290	3.71×10^{-2}	0.897	1.92	0.34	0.999
NIP	Temp. (°C)							
	15	0.32	0.108	9.90×10^{-3}	0.805	0.31	0.42	0.999
	25	0.36	0.209	2.74×10^{-2}	0.981	0.38	0.25	0.999
	35	0.38	0.256	3.37×10^{-2}	0.955	0.40	0.24	0.998
	C_0 (mg/L)							
	3.0	0.36	0.209	2.74×10^{-2}	0.981	0.38	0.25	0.999
	5.0	0.40	0.270	3.24×10^{-2}	0.933	0.42	0.24	0.998
	8.0	0.46	0.192	1.88×10^{-2}	0.988	0.47	0.24	0.999

from the liquid phase up to the solid phase boundary [33]:

$$\ln(1 - F) = -k_f t \quad (10)$$

F is the fractional attainment of equilibrium ($F = q_t/q_e$), k_f (cm/s) is the film diffusion rate constant.

For a solid–liquid adsorption process, the solute transfer is usually characterized by either external mass transfer (boundary layer diffusion) for nonporous media or intraparticle diffusion for porous matrices, or both combined. When Pb(II) ion solution was mixed with the adsorbent, transport of the Pb(II) ions from the solution through the interface between the solution and the adsorbent and into the particle pores may effective [39]. One of these steps may be the rate control step. If the intercept of plot q_t *vs.* $t^{1/2}$ passed through the origin, then intraparticle diffusion is the sole rate-limiting step. While the plot of $-\ln(1 - F)$ *vs.* t with zero intercept would suggest that the kinetics of the adsorption process is controlled by diffusion through the liquid film [40]. As shown in Table 4, intercept of plot of q_t *vs.* $t^{1/2}$ (y) passed through closely from the origin, which indicated the boundary layer effect. However the intercept of plot of $-\ln(1 - F)$ *vs.* t was larger, which suggested that intraparticle diffusion was involved in the sorption process but it is not the only rate-limiting mechanism.

The pore diffusion coefficients for intraparticle transport and the film diffusion coefficients for external mass transfer can be described using following equation [41,42]:

$$D_p = 0.03 r_0^2 / t_{1/2} \quad (11)$$

$$D_f = 0.23 (r_0 \delta q_e) / t_{1/2} \quad (12)$$

D_p (cm^2/s) and D_f (cm^2/s) are the pore diffusion coefficient and the film diffusion coefficient, respectively. r_0 (cm) is the radius of sorbent and $t_{1/2}$ (min) is the time for half of the adsorption. r_0 value obtained of Pb(II)-IIP synthesized in the present work was 1.255×10^{-4} cm. δ (cm) is the film thickness. Assuming spherical geometry for the sorbent, thickness of the film is taken as 10^{-3} cm, as reported by earlier workers [43].

According to Argun et al. [42], for pore diffusion to be rate-limiting, the values of D_p should be in the range of 10^{-11} to 10^{-13} cm^2/s. For film diffusion to be rate-limiting, the values of D_f should be in the range of 10^{-6} to 10^{-8} cm^2/s. From these parameters in Table 4, it can be concluded that pore diffusion was more dominant than film diffusion.

As a result, the kinetics of interaction of Pb(II) with the Pb(II)-IIP surfaces are not overwhelmingly controlled by any one mechanism. Although second-order mechanism and pore diffusion are more likely, contributions from first-order as well as from external diffusion could not be completely ruled out.

3.3.4. Adsorption isotherms

Adsorption isotherm experiments were carried out at different temperatures. As shown in Fig. 6, the curves indicated that the adsorption amount increased sharply in initial concentration, but after a certain concentration, it approached saturation. And the maximum adsorption capacity decreased with temperature on Pb(II)-IIP while increased on NIP. Compared with NIP, the adsorption capacity of Pb(II) on Pb(II)-IIP was near two times of NIP.

Subsequently, two isotherms-Langmuir and Freundlich used to analyze the equilibrium experimental data.

Langmuir isotherm assumes monolayer adsorption onto a surface with a finite number of identical sites [44]. It was expressed as follows:

$$\frac{C_e}{q_e} = \frac{1}{q_m b} + \frac{C_e}{q_m} \quad (13)$$

Table 4
Intraparticle mass transfer, external mass transfer parameters for adsorption of Pb(II) onto Pb(II)-IIP.

Parameter	Intraparticle mass transfer			External mass transfer		
	k_d (mg/g min$^{1/2}$)	y	D_p (cm^2/s)	k_f (cm/s)	Intercepts	D_f (cm^2/s)
Temp. (°C)						
15	1.56×10^{-2}	0.628	1.89×10^{-11}	5.05×10^{-2}	1.792	8.66×10^{-10}
25	2.05×10^{-2}	0.579	2.36×10^{-11}	5.62×10^{-2}	2.173	1.07×10^{-9}
35	1.86×10^{-2}	0.537	1.58×10^{-11}	7.51×10^{-2}	1.396	6.54×10^{-9}
C_0 (mg/L)						
3.0	2.05×10^{-2}	0.579	2.36×10^{-11}	5.62×10^{-2}	2.173	1.07×10^{-9}
5.0	1.81×10^{-2}	1.020	1.58×10^{-11}	1.74×10^{-2}	2.249	1.10×10^{-9}
8.0	3.90×10^{-2}	1.564	1.05×10^{-11}	3.71×10^{-2}	1.878	1.20×10^{-9}

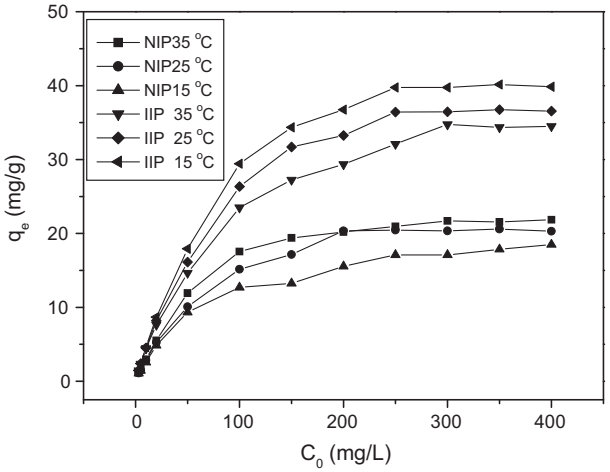

Fig. 6. Adsorption isotherms for adsorption of Pb(II) onto Pb(II)-IIP and NIP at different temperatures.

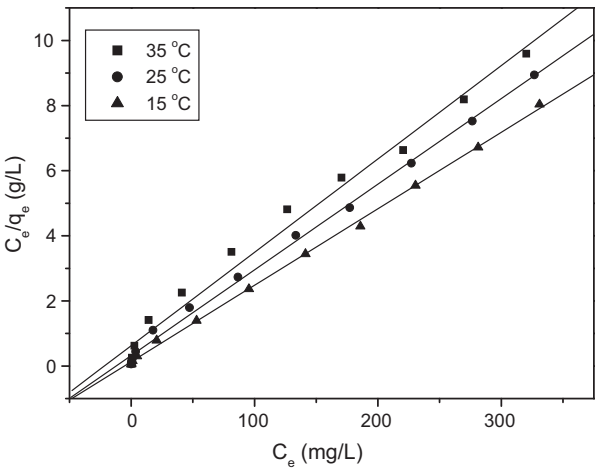

Fig. 7. Simulation for adsorption of Pb(II) onto Pb(II)-IIP using Langmuir model.

b (L/mg) and q_m (mg/g) are the Langmuir coefficients, representing the adsorption equilibrium constant and the monolayer capacity, respectively.

A dimensionless constant separation factor was denoted as R_L:

$$R_L = \frac{1}{1 + bC_0} \tag{14}$$

The R_L value indicates whether the type of the isotherm is favorable ($0 < R_L < 1$), unfavorable ($R_L > 1$), linear ($R_L = 1$), or irreversible ($R_L = 0$) [45].

Freundlich isotherm is an empirical equation based on adsorption on a heterogeneous surface [46]. The equation is commonly represented by:

$$\ln q_e = \ln K_F + \frac{1}{n} \ln C_e \tag{15}$$

K_F (mg/g (L/mg)$^{1/n}$) and n are the Freundlich constants characteristics of the system, indicating the adsorption capacity and the adsorption intensity, respectively. If the value of $1/n$ is lower than 1, it indicates a normal Langmuir isotherm; otherwise, it is indicative of cooperative adsorption.

The Langmuir and Freundlich adsorption constants and the corresponding correlation coefficients are listed in Table 5. The adsorption of Pb(II) on Pb(II)-IIP was well fitted to the Langmuir isotherm model with the higher R^2 (0.999–0.984) (linear plot was shown in Fig. 7). It indicated the adsorption took place at specific homogeneous sites within the adsorbent forming monolayer coverage of Pb(II) ions at the surface of the sorbent. Furthermore, the values of R_L for the Langmuir isotherm were between 0 and 1, and the Freundlich constant $1/n$ was smaller than 1, indicating a favorable process.

The observed decrease in the adsorption capacity with an increase of temperature indicated that low temperature was in favor of Pb(II) ions adsorption onto Pb(II)-IIP. This may be due to a tendency for the Pb(II) ions to escape from the solid phase to the bulk phase with an increase in the temperature of the solutions. This effect suggested weakening of adsorptive forces between the active sites of the adsorbent and adsorbate species and also between the adjacent molecules of the adsorbed phase with the rise of temperature [47]. As a result, it showed that Pb(II) adsorption onto Pb(II)-IIP was of a chemical together with a physical property, which is usually associated with low adsorption heat [48]. On the one hand, Pb(II) chelated with metal-binding groups (–OH, $-NH_2$) on Pb(II)-IIP; on the other hand, specific cavities that complementary to the imprint ion in size, shape and coordination geometries on imprinted polymer offer perfect matched physical adsorption sites. As for NIP, it was assumed one simple chemical reaction mechanism, and that rise of temperature favored the sorbate transport to the sorbent, and that increase in the number of the sorption sites generated because of breaking of some internal bonds near the edge of active surface sites of sorbent [49].

A comparison based on Langmuir saturation adsorption capacity for Pb(II), it indicated that the imprinted polymer supported by SBA-15 (38.01 mg/g) was much more efficient than NIP (18.4 mg/g). Moreover, the saturation adsorption capacity in present work is higher than the values reported for Pb(II) adsorption on Pb(II)-IIP prepared by bulk polymerization (2.01 mg/g) [50], Pb(II)-imprinted amino-functionalized silica gel (19.66 mg/g) [51] and Pb(II)-IIP on nano-TiO_2 matrix (22.70 mg/g) [52], respectively. The high adsorption capacity in this paper can be explained as follows: the polymer grafted onto the surface of the inner channel of large surface area SBA-15, after leached of Pb(II), enough cavities left on the surface of polymer. As a novel supported matrix applied in surface imprinted system, SBA-15 based imprinted polymer shows great potential in the separation of metal ions.

3.3.5. The thermodynamic parameters

In environmental engineering practice, both energy and entropy factors must be considered in order to determine which process will occur spontaneously. The thermodynamic parameters can be

Table 5
The comparison of the Langmuir and Freundlich isotherm parameters obtained from adsorption isotherms for adsorption of Pb(II) onto Pb(II)-IIP at different temperatures.

Temp. (°C)	Langmuir				Freundlich		
	q_m (mg/g)	K (L/mg)	R^2	R_L	K_F	n	R^2
15	42.55	1.81×10^{-1}	0.999	0.6479–0.0136	5.06	2.486	0.980
25	38.01	8.15×10^{-2}	0.997	0.8035–0.0298	4.49	2.487	0.987
35	34.86	3.02×10^{-2}	0.984	0.8788–0.0516	3.96	2.483	0.993

Table 6
Thermodynamic parameters for the adsorption of Pb(II) onto Pb(II)-IIP and NIP.

Polymer	C_0 (mg/L)	ΔH° (kJ/mol)	ΔS° (J/mol k)	ΔG° (kJ/mol)		
				15 °C	25 °C	35 °C
Pb(II)-IIP	100.0	−17.69	−6.79	−15.73	−15.67	−15.59
	200.0	−12.35	4.32	−13.59	−13.64	−13.68
	300.0	−6.62	20.12	−12.42	−12.62	−12.82
NIP	100.0	10.14	70.09	−10.05	−10.75	−11.45
	200.0	11.89	79.31	−10.95	−11.75	−12.54
	300.0	31.71	152.28	−12.15	−13.67	−15.19

Table 7
Competitive sorption of different ions by Pb(II)-IIP and NIP sorbent (experimental conditions: initial concentrations of metal ions: 5.0 mg/L; Pb(II)-IIP 0.08 g; shaking time 10 min; adsorption time 90 min; temperature 25 °C).

Metal type	SBA-15		Pb(II)-IIP		NIP		k'
	k_d (mL/g)	k	k_d (mL/g)	k	k_d (mL/g)	k	
Pb(II)	742.82		330.27		124.16		
Cr(III)	308.44	2.41	26.06	12.67	108.59	1.14	11.08
Co(II)	143.63	5.17	0.78	422.56	101.50	1.22	345.44
Cu(II)	207.55	3.58	23.79	13.88	81.98	1.51	9.17
Hg(II)	226.82	3.27	26.85	12.30	22.33	5.56	2.21
Mg(II)	197.66	3.76	19.41	17.02	78.17	1.59	10.71
Ni(II)	204.31	3.64	9.03	36.56	46.88	2.65	13.80
Zn(II)	222.74	3.33	16.01	20.63	113.42	1.09	18.85

obtained using the following equation [53]:

$$\ln K_D = -\frac{\Delta H^\circ}{RT} + \frac{\Delta S^\circ}{R} \quad \text{(kJ/mol)} \tag{16}$$

$$\Delta G^\circ = \Delta H^\circ - T\,\Delta S^\circ \quad \text{(kJ/mol)} \tag{17}$$

where R is the universal gas constant, T (K) is the temperature. Moreover, K_D is the equilibrium constant ($K_D = q_e/C_e$). Table 6 summarizes the values of these thermodynamic parameters.

The negative values of ΔG° indicate the spontaneous nature of adsorption process. When the initial concentration increased from 100.0 to 300.0 mg/L, the free energy change shifts to low negative value, suggested that the adsorption was more spontaneous at low concentration. Negative value of ΔH° indicated that the binding of Pb(II) ions was exothermic in nature. In addition, the negative value of ΔS° at low initial concentration indicated that disorder of the system decreased during adsorption process; while the positive entropy value at the initial concentration of 200.0, 300.0 mg/L suggested an increase in the randomness at the solid/solution interface during the adsorption process.

Compared with ΔG° for the adsorption of Pb(II) on NIP, the adsorptive forces were stronger on Pb(II)-IIP indicating more spontaneous thermodynamically process due to the specific recognition sites on Pb(II)-IIP. In addition, the value of ΔH° on NIP was positive, indicating that the binding of Pb(II) ions was endothermic.

3.3.6. Selectivity study

Competitive adsorption of the same charge or similar ionic radius ions such as Pb(II)/Cr(III), Pb(II)/Co(II), Pb(II)/Cu(II), Pb(II)/Hg(II), Pb(II)/Mg(II), Pb(II)/Ni(II), and Pb(II)/Zn(II) from their mixtures were investigated by using SBA-15, Pb(II)-IIP and NIP, respectively. As shown in Table 7, the $K_{d(\mathrm{IIP})}$ value of Pb(II)-IIP for Pb(II) were larger, while $K_{d(\mathrm{IIP})}$ decreased significantly for Cr(III), Co(II), Cu(II), Hg(II), Mg(II), Ni(II), and Zn(II). SBA-15 has low k value due to strong physical adsorption towards variety metal ions without selectivity, while NIP has low k value due to have random distribution of ligand functionalities in the polymeric network, whereas in the case of Pb(II)-IIP, the cavities created after removal of the template were complementary to the imprint ion in size, shape and coordination geometries. It demonstrated that Pb(II)-IIP synthesized for Pb(II) had a higher selectivity specialism for this ion.

4. Conclusions

A novel high ordered mesoporous Pb(II)-imprinted polymer grafted on mesoporous material SBA-15 has been first synthesized through a simple surface imprinting technology. The graft occurred on the surface of the inner channel, therefore the polymer exhibited fast kinetics and high adsorption capacity for Pb(II). The adsorption behavior of Pb(II) onto Pb(II)-IIP belonged to the pseudo-second-order kinetic model and the adsorption process was a chemical process. Langmuir was well fitted with the data and indicated the formation of monolayer coverage of Pb(II) ions at the surface of the sorbent. Thermodynamic parameters indicated the adsorption process was spontaneous, exothermic and good affinity nature. Competitive adsorption studies showed that Pb(II)-IIP offers the advantages of selectivity toward targeted Pb(II) compared with raw SBA-15 and NIP even in the presence other metal ions.

Acknowledgements

This work was financially supported by the National Natural Science Foundation of China (Nos.20877036 and 21077046), Ph.D. Innovation Programs Foundation of Jiangsu University (No. CX09B_12XZ).

References

[1] M.K. Aroua, S.P.P. Leong, L.Y. Teo, C.Y. Yin, W.M.A.W. Daud, Real-time determination of kinetics of adsorption of lead(II) onto palm shell-based activated carbon using ion selective electrode, Bioresour. Technol. 99 (2008) 5786–5792.
[2] B.L. Martins, C.C.V. Cruz, A.S. Luna, C.A. Henriques, Sorption and desorption of Pb^{2+} ions by dead Sargassum sp. Biomass, Biochem. Eng. J. 27 (2006) 310–314.
[3] L. Wang, J. Zhang, R. Zhao, Y. Li, C. Li, C.L. Zhang, Adsorption of Pb(II) on activated carbon prepared from Polygonum orientale Linn.: kinetics, isotherms, pH, and ionic strength studies, Bioresour. Technol. 101 (2010) 5808–5814.
[4] J.Y. Pan, S. Wang, R.F. Zhang, A novel Pb(II)-imprinted IPN for selective preconcentration of lead from water and sediments, Int. J. Environ. Anal. Chem. 86 (2006) 855–865.
[5] E.M. Thurman, M.S. Mills, Solid-phase Extraction, Principles and Practice, Wiley, New York, 1998.

[6] M. Ghaedi, F. Ahmadi, Z. Tavakoli, M. Montazerozohori, A. Khanmohammadi, M. Soylak, Three modified activated carbons by different ligands for the solid phase extraction of copper and lead, J. Hazard. Mater. 152 (2008) 1248–1255.
[7] H. Nishide, J. Deguchi, E. Tsuchida, Selective adsorption of metal ions on crosslinked poly(vinylpyridine) resin prepared with a metal ion as a template, Chem. Lett. 5 (1976) 169–174.
[8] Q. He, X.J. Chang, Q. Wu, X.P. Huang, Z. Hu, Y.H. Zhai, Synthesis and applications of surface-grafted Th(IV)-imprinted polymers for selective solid-phase extraction of thorium(IV), Anal. Chim. Acta 605 (2007) 192–197.
[9] F.Q. An, B.J. Gao, X.Q. Feng, Adsorption and recognizing ability of molecular imprinted polymer MIP-PEI/SiO_2 towards phenol, J. Hazard. Mater. 157 (2008) 286–292.
[10] H.H. Yang, S.Q. Zhang, F. Tan, Z.X. Zhuang, X.R. Wang, Surface molecularly imprinted nanowires for biorecognition, J. Am. Chem. Soc. 127 (2005) 1378–1379.
[11] B.J. Gao, J. Wang, F.Q. An, Q. Liu, Molecular imprinted material prepared by novel surface imprinting technique for selective adsorption of pirimicarb, Polymer 49 (2008) 1230–1238.
[12] F. Bonini, S. Piletsky, A.P.F. Turner, A. Speghini, A. Bossi, Surface imprinted beads for the recognition of human serum albumin, Biosens. Bioelectron. 22 (2007) 2322–2328.
[13] W. Luo, L.H. Zhu, C. Yu, H.Q. Tang, H.X. Yu, X. Li, X. Zhang, Synthesis of surface molecularly imprinted silica micro-particles in aqueous solution and the usage for selective off-line solid-phase extraction of 2,4-dinitrophenol from water matrixes, Anal. Chim. Acta. 618 (2008) 147–156.
[14] P. Kumar, V.V. Guliants, Periodic mesoporous organic–inorganic hybrid materials: applications in membrane separations and adsorption, Micropor. Mesopor. Mater. 132 (2010) 1–14.
[15] L.C.C. Silva, L.B.O. Santos, G. Abate, I.C. Cosentino, M.C.A. Fantini, J.C. Masini, J.R. Matos, Adsorption of Pb^{2+}, Cu^{2+} and Cd^{2+} in FDU-1 silica and FDU-1 silica modified with humic acid, Microporous Mesoporous Mater. 110 (2008) 250–259.
[16] A. Heidari, H. Younesi, Z. Mehraban, Removal of Ni(II), Cd(II), and Pb(II) from a ternary aqueous solution by amino functionalized mesoporous and nano mesoporous silica, Chem. Eng. J. 153 (2009) 70–79.
[17] C.X. Song, X.L. Zhang, C.Y. Jia, P. Zhou, X. Quan, C.Y. Duan, Highly sensitive and selective fluorescence sensor based on functional SBA-15 for detection of Hg^{2+} in aqueous media, Talanta 81 (2010) 643–649.
[18] A.M. Liu, K. Hidajat, S. Kawi, D.Y. Zhao, A new class of hybrid mesoporous materials with functionalized organic monolayers for selective adsorption of heavy metal ions, Chem. Commun. 13 (2000) 1145–1146.
[19] H. Huang, C. Yang, H. Zhang, M. Liu, Preparation and characterization of octyl and octadecyl-modified mesoporous SBA-15 silica molecular sieves for adsorption of dimethyl phthalate and diethyl phthalate, Microporous Mesoporous Mater. 111 (2008) 254–259.
[20] X.M. Xue, F.T. Li, Removal of Cu(II) from aqueous solution by adsorption onto functionalized SBA-16 mesoporous silica, Microporous Mesoporous Mater. 116 (2008) 116–122.
[21] J. Li, T. Qi, L. Wang, C. Liu, Y. Zhang, Synthesis and characterization of imidazole-functionalized SBA-15 as an adsorbent of hexavalent chromium, Mater. Lett. 61 (2007) 3197–3200.
[22] J.N. Zhang, Z. Ma, J. Jiao, H.F. Yin, W.F. Yan, E.W. Hagaman, J.H. Yu, S. Dai, Layer-by-layer grafting of titanium phosphate onto mesoporous silica SBA-15 surfaces: synthesis, characterization, and applications, Langmuir 25 (2009) 12541–12549.
[23] N.V Majeti, K. Ravi, A review of chitin and chitosan applications, React. Funct. Polym. 46 (2000) 1–27.
[24] N. Viswanathan, C.S. Sundaram, S. Meenakshi, Sorption behaviour of fluoride on carboxylated cross-linked chitosan beads, Colloids Surf., B. 68 (2009) 48–54.
[25] F. Xi, J. Wu, Macroporous chitosan layer coated on non-porous silica gel as a support for metal chelate affinity chromatographic adsorbent, J. Chromatogr. A 1057 (2004) 41–47.
[26] Q.H. Shi, Y. Tian, X.Y. Dong, S. Bai, Y. Sun, Chitosan-coated silica beads as immobilized metal affinity support for protein adsorption, Biochem. Eng. J. 16 (2003) 317–322.
[27] D.Y. Zhao, J.L. Feng, Q.S. Huo, N. Melosh, G.H. Fredrikson, B.F. Chmelka, G.D. Stucky, Triblock copolymer syntheses of mesoporous silica with periodic 50 to 300 angstrom pores, Science 279 (1998) 548–552.
[28] S. Dai, M.C. Burleigh, Y.S. Shin, C.C. Morrow, C.E. Barnes, Z.L. Xue, Imprint coating: a novel synthesis of selective functionalized ordered mesoporous sorbents, Angew. Chem. Int. Ed. Engl. 38 (1999) 1235–1239.
[29] R. Yueming, Z. Milin, Z. Dan, Synthesis and properties of magnetic Cu(II) ion imprinted composite adsorbent for selective removal of copper, Desalination 228 (2008) 135–149.
[30] D.W. Ren, D.C. Bao, W.L. Wang, X.J. Ma, Study on N-acetylated chitosans by FTIR and XRD, Spectral. Anal. 26 (2006) 1217–1220.
[31] D. Pérez-Quintanilla, A. Sánchez, I.D. Hierro, M. Fajardo, I. Sierra, Preparation, characterization, and Zn^{2+} adsorption behavior of chemically modified MCM-41 with 5-mercapto-1-methyltetrazole, J. Colloid Interface Sci. 313 (2007) 551–562.
[32] L. Zhao, S. Wang, Y. Wu, Q. Hou, Y. Wang, S. Jiang, Salicylidene schiff base assembled with mesoporous Silica SBA-15 as hybrid materials for molecular logic function, J. Phys. Chem. C 111 (2007) 18387–18391.
[33] S.S. Gupta, K.G. Bhattacharyya, Adsorption of Ni(II) on clays, J. Colloid Interface. Sci. 295 (2006) 21–32.
[34] L. Wang, R. Xing, S. Liu, Y. Qin, K. Li, H. Yu, R. Li, P. Li, Studies on adsorption behavior of Pb(II) onto a thiourea-modified chitosan resin with Pb(II) as template, Carbohydr. Polym. 81 (2010) 305–310.
[35] C.A. Quirarte-Escalante, V. Soto, W. Cruz, G.R. Porras, R.M.S. Gomez-Salazar, Synthesis of hybrid adsorbents combining sol-gel processing and molecular imprinting applied to lead removal from aqueous streams, Chem. Mater. 21 (2009) 1439–1450.
[36] V. Sarin, K.K. Pant, Removal of chromium from industrial waste by using eucalyptus bark, Bioresour. Technol. 97 (2006) 15–20.
[37] A.R. Iftikhar, H.N. Bhatti, M.A. Hanifa, R. Nadeem, Kinetic and thermodynamic aspects of Cu(II) and Cr(III) removal from aqueous solutions using rose waste biomass, J. Hazard. Mater. 161 (2009) 941–947.
[38] M. Özacara, I.A. Sengilb, H.J. Türkmenler, Equilibrium and kinetic data, and adsorption mechanism for adsorption of lead onto valonia tannin resin, Chem. Eng. J. 143 (2008) 32–42.
[39] G. Mckay, The adsorption of basic dye onto silica from aqueous solution-solid diffusion model, Chem. Eng. Sci. 39 (1984) 129–138.
[40] A. Ozcan, A.S. Ozcan, Adsorption of Acid Red 57 from aqueous solutions onto surfactant-modified sepiolite, J. Hazard. Mater. 125 (2005) 252–259.
[41] M.E. Argun, S. Dursun, A new approach to modification of natural adsorbent for heavy metal adsorption, Bioresour. Technol. 99 (2008) 2516–2527.
[42] M.E. Argun, S. Dursun, M. Karatas, M. Gürü, Activation of pine cone using Fenton oxidation for Cd(II) and Pb(II) removal, Bioresour. Technol. 99 (2008) 8691–8698.
[43] K.G. Varshney, A.A. Khan, U. Gupta, S.M. Maheshwari, Kinetics of adsorption of phosphamidon on antimony (V) phosphate cation exchanger: evaluation of the order of reaction and some physical parameters, Colloids. Surf. A: Physicochem. Eng. Asp. 113 (1996) 19–23.
[44] E. Demirbas, N. Dizge, M.T. Sulak, M. Kobya, Adsorption kinetics and equilibrium of copper from aqueous solutions using hazelnut shell activated carbon, Chem. Eng. J. 148 (2009) 480–487.
[45] S. Azizian, Kinetic models of sorption: a theoretical analysis, J. Colloid Interface Sci. 276 (2004) 47–52.
[46] N.Y. Mezenner, A. Bensmaili, Kinetics and thermodynamic study of phosphate adsorption on iron hydroxide-eggshell waste, Chem. Eng. J. 147 (2009) 87–96.
[47] K.K. Singh, M. Talat, S.H. Hasan, Removal of lead from aqueous solutions by agricultural waste maize bran, Bioresour. Technol. 97 (2006) 2124–2130.
[48] S. Karaca, A. Gürses, M. Ejder, M. Aēlkylldlz, Adsorptive removal of phosphate from aqueous solutions using raw and calcinated dolomite, J. Hazard. Mater. 6 (2006) 273–279.
[49] J. Acharyaa, J.N. Sahub, C.R. Mohantyc, B.C. Meikap, Removal of lead(II) from wastewater by activated carbon developed from Tamarind wood by zinc chloride activation, Chem. Eng. J. 149 (2009) 249–262.
[50] C. Esen, M. Andac, N. Bereli, R. Say, E. Henden, A. Denizli, Highly selective ion-imprinted particles for solid-phase extraction of Pb^{2+} ions, Mater. Sci. Eng. C 29 (2009) 2464–2470.
[51] X. Zhu, Y. Cui, X. Chang, X. Zou, Z. Li, Selective solid-phase extraction of lead(II) from biological and natural water samples using surface-grafted lead(II)-imprinted polymers, Microchim. Acta 164 (2009) 125–132.
[52] C. Li, J. Gao, J. Pan, Z. Zhang, Y. Yan, Synthesis, characterization, and adsorption performance of Pb(II)-imprinted polymer in nano-TiO_2 matrix, J. Environ. Sci. 21 (2009) 1722–1729.
[53] J.C.Y. Ng, W. Cheung, G. McKay, Equilibrium studies of the sorption of Cu(II) ions onto chitosan, J. Colloid. Interface Sci. 255 (2002) 64–74.